# Wave propagation and structural dynamics in graphene nanoribbons

F Scarpa[1], M Ruzzene[2], S Adhikari[3], R Chowdhury[3]

[1]Advanced Composites Centre for Innovation and Science, University of Bristol, BS8 1TR Bristol, UK

[2]School of Aerospace Engineering, Georgia Institute of Technology, Atlanta, GA 30332

[3]Multidisciplinary Nanotechnology Centre, Swansea University, Singleton Park, SA2 8PP Swansea, UK

## ABSTRACT

Graphene nanoribbons (GNRs) are novel interesting nanostructures for the electronics industry, whereas their state as metallic or semiconductor material depends on the chirality of the graphene. We model the natural frequencies and the wave propagation characteristics of GNRs using an equivalent atomistic-continuum FE model previously developed by some of the Authors, where the C-C bonds thickness and average equilibrium lengths during the dynamic loading are identified through the minimisation of the system Hamiltonian. A molecular mechanics model based on the UFF potential is used to benchmark the hybrid FE models developed. The wave dispersion characteristics of the GNRs are simulated using a Floquet-based wave technique used to predict the pass-stop bands of periodic structures. We demonstrate that the thickness and equilibrium lengths for the different dynamic cases are different from the classical constant values used in open literature (0.34 nm for thickness and 0.142 nm for equilibrium length), in particular when considering out-of-plane flexural deformations. These parameters have to be taken into account when nanoribbons are designed as nano-oscillators.

## 1. INTRODUCTION

Since their inception as theoretical concepts,[1] graphene nanoribbons (GNRs) have attracted a sustained interest in the nanoelectronics community as possible replacements to silicon semiconductors, and potential quasi-THz oscillators and quantum dots.[2] The electronic state of GNRs depend significantly on the edge structure. The zigzag layout provides the edge localized state with non-bonding molecular orbitals near the Fermi energy, with induced large changes in optical and electronic properties from quantization. DFT calculations and experimental measurements have shown that zigzag edge GNRs are always metallic, while armchair nanoribbons are semiconducting with an energy gap decreasing with the increase of the GNR width.[3,4] GNRs have been also prototyped as photonics waveguides,[5] and recently proposed for thermal phononics to control the reduction of thermal conductivity.[6]

In this work, we present the results related to the natural frequencies and wade dispersion characteristics of graphene nanoribbons considered as periodic structures. In structural dynamics design, the wave propagation characteristics of periodic systems (both 1D and 2D) have been extensively used to tune the acoustic and vibrational signature of structures, materials and sensors,[7–9] while at nanoscale level the periodicity of nanotubes array has also been used to develop nanophotonics crystals.[10] The nanoribbon models we introduce are developed using a hybrid atomistic continuum FE representation, where the covalent bonds are represented as Timoshenko beams with equivalent mechanical properties (Young's modulus, Poisson's ratio) derived by the minimisation of the Hamiltonian, or total potential energy for the static case.[11–13] The equivalent mechanical properties for the $sp^2$ C-C bond are expressed in terms of the thickness of the bond itself. It is useful to remember that there is nor physical thickness *per se* for the covalent bonds, neither for the carbon atoms involved. Nonetheless, the nanostructure subjected to a mechanical static loading tends to reach its equilibrium state corresponding to the minimum potential energy. The geometric and material configuration of the equivalent continuum mechanics structures (plate and/or hollow tube) will be therefore defined by the energy equilibrium conditions of the

nanostructure, and cannot be ascribed as fixed. The length of the covalent bonds merits also some considerations. In finite size rectangular SLGS, the lengths of the C-C bonds at the equilibrium after loading are unequal, ranging between 0.136 nm and 0.144 nm, and depend on the type of loading, size and boundary conditions of the mechanical case,[14,15] and the location of the SLGS itself (i.e., the edges[16]). This fact contrasts with the classical use of the fixed value of 0.142 nm at equilibrium considered in most mechanical simulations.[17–20] The variation of thickness and distributions of equilibrium length are important factors to consider when computing the *homogenised* mechanical properties of the graphene - i.e., the equivalent mechanical performance of the graphene as a *continuum*. Homogenization theory applied to periodic structures dictates a minimum number of periodic elements to identify asymptotic values for the linear elastic mechanical properties (stiffness, Poisson's ratios).[21,22] However, the variability of thickness and equilibrium lengths over the same graphene sheets when subjected to different loading conditions will result into different averaged homogenised mechanical properties according to the test cases. Our approach is to model the graphene and nanoribbons as a structure*s*, not as an equivalent continuum material.

## 2. MODELLING

We use the atomistic-continuum equivalence model for the $sp^2$ carbon-carbon bonds to extract the equivalent isotropic mechanical properties (Young's modulus and Poisson's ratio) as a functions of the thickness $d$ of the C-C bond.[11,13] The model is based on the equivalence between the harmonic potential provided by force models such as AMBER or linearised Morse, and the strain energies associated to out-of-plane torsional, axial and bending deformation of a deep shear Timoshenko beam:

$$\begin{array}{c} \frac{k_r}{2}\left(\Delta r\right)^2 = \frac{EA}{2L}\left(\Delta r\right)^2 \\ \frac{k_\tau}{2}\left(\Delta \varphi\right)^2 = \frac{GJ}{2L}\left(\Delta \varphi\right)^2 \\ \frac{k_\theta}{2}\left(\Delta \theta\right)^2 = \frac{EI}{2L}\frac{4+\Phi}{1+\Phi}\left(\Delta \theta\right)^2 \end{array} \tag{1}$$

The first row of (1) corresponds to the equivalence between stretching and axial deformation mechanism (with $E$ being the equivalent Young's modulus), while the second one equates the torsional deformation of the C-C bond with the pure shear deflection of the structural beam associated to an equivalent shear modulus $G$. Contrary with similar approaches previously used,[18,20] the term equating the in-plane rotation of the C-C bond (third row of 1) is equated to a bending strain energy related to a deep shear beam model, to take into account the shear deformation of the cross section. The shear correction term becomes necessary when considering beams with aspect ratio lower than 10.[23] For circular cross sections, the shear deformation constant can be expressed as:[11]

$$\Phi = \frac{12EI}{GA_sL^2} \tag{2}$$

In (2), $A_s = A/F_s$ is the reduced cross section of the beam by the shear correction term $F_s$:[24]

$$F_s = \frac{6+12\nu+6\nu^2}{7+12\nu+4\nu^2} \tag{3}$$

The insertion of (2) and (3) in (1) leads to an nonlinear relation between the thickness $d$ and the Poisson's ratio $\nu$ of the equivalent beam:[11]

$$k_\theta = \frac{k_r d^2}{16}\frac{4A+B}{A+B} \tag{4}$$

Where:

$$A = 112L^2k_\tau + 192L^2k_\tau\nu + 64L^2k_\tau\nu^2 \tag{5}$$

$$B = 9k_rd^2 + 18k_rd^4\nu + 9k_rd^4\nu^2 \tag{6}$$

The values for the force constants for the AMBER model are $k_r = 6.52\times10^{-7}\mathrm{N\,mm^{-1}}$, $k_\theta = 8.76\times10^{-10}\mathrm{N\,nm\,rad^{-2}}$, and $k_\tau = 2.78\times10^{-10}\mathrm{N\,nm^{-1}\,rad^{-2}}$. The equivalent mechanical properties of the C-C bond can be determined performing a nonlinear optimisation of (1) using a Marquardt algorithm. The C-C bond can then be discretised as a single two-nodes three dimensional Finite Element (FE) model beam with a $6\times6$ stiffness matrix $[\mathbf{K}]_\mathbf{e}$

described in,[25] where the nodes represent the atoms. The mass matrix $[\mathbf{M}]_\mathbf{e}$ of the bond is represented through a lumped matrix approach:[26]

$$[\mathbf{M}]_\mathbf{e} = diag\left[\begin{array}{cccccc} \frac{m_c}{3} & \frac{m_c}{3} & \frac{m_c}{3} & 0 & 0 & 0 \end{array}\right] \tag{7}$$

Where $m_c = 1.9943 \times 10^{-26} kg$. The elemental matrices are then assembled in the usual Finite Element fashion as global stiffness and mass matrices $[\mathbf{K}]$ and $[\mathbf{M}]$ respectively. The undamped eigenvalue problem $\left([\mathbf{K}] - \omega^2 [\mathbf{M}]\right) \{\mathbf{x}\} = \{\mathbf{0}\}$ is solved using a classical Block Lanczos algorithm implemented in the commercial FE code ANSYS (Rel. 12). According to Eqs. (2 - 4), the natural frequencies $\omega_i$ are however dependent on the thickness $d$. In the hybrid FE simulation, we consider also the variation of the bond length $l$ across the graphene sheet, a phenomenon observed in several models of SLGSs subjected to mechanical loading.[11,14,16,27] To identify a unique set of thickness and equilibrium lengths for a specific eigensolution, one needs to minimize the Hamiltonian of the system:[28]

$$H = T + U \tag{8}$$

Where $T$ and $U$ are the kinetic and strain energy of the system respectively. Using the mass-normalized normal modes $[\mathbf{\Phi}]$ associated to the eigenvalue problem[29] , the Hamiltonian (8) for each eigensolution $i$ can be rewritten as:

$$H_i = \frac{1}{2} \{\mathbf{\Phi}\}_i^T [\mathbf{M}] \{\mathbf{\Phi}\}_i \times \omega_i^2 + \frac{1}{2} \{\Phi\}_i^T [\mathbf{K}] \{\Phi\}_i = \omega_i^2 \tag{9}$$

The hybrid FE simulations have been benchmarked against a Molecular Mechanics approach developed by some of the Authors for the vibration of ZnO nanotubes.[30] The total energy of the $sp^2$ C-C bond expressed with the UFF potential[31] is used to create the Hessian matrix of the minimized system, the eigenvalues of the latter being the analogous of the natural frequencies obtained from the FE representation.

The 1D wave propagation analysis is carried out using a technique implemented by.[9,32] Applying the Floquet conditions between the left and right nodal degrees of freedom (DOFs) $\{\mathbf{u}\}^L$ and $\{\mathbf{u}\}^R$ one obtains:

$$\{\mathbf{u}\}^L = e^{-ik_x} \{\mathbf{u}\}^R \tag{10}$$

Where $-\pi \leq k_x \leq \pi$ is the propagation constant within the first Brillouin zone.[33] The generalised DOFs of the system will be in general complex (real and imaginary part), while for travelling waves the propagation constant $k_x$ will be real. Eq. (10) can be therefore recast as:

$$\begin{array}{l} \{\mathbf{u}\}^L_{\mathrm{Im}} = \{\mathbf{u}\}^R_{\mathrm{Im}} \cos k_x - \{\mathbf{u}\}^R_{\mathrm{Re}} \sin k_x \\ \{\mathbf{u}\}^L_{\mathrm{Re}} = \{\mathbf{u}\}^R_{\mathrm{Im}} \cos k_x + \{\mathbf{u}\}^R_{\mathrm{Re}} \sin k_x \end{array} \tag{11}$$

The real and imaginary parts of the domain in the FE representation are produced creating two superimposed meshes, linked by the boundary conditions (11). For a given wave propagation constant $k_x$, the resultant eigenvalue problem provides thefrequency associated to the wave dispersion curve. Similarly to the undamped eigenvalue problem, the minimisation of the Hamiltonian (9) is carried out to identify the set of thickness and average bond length required for the eigenvalue solution.

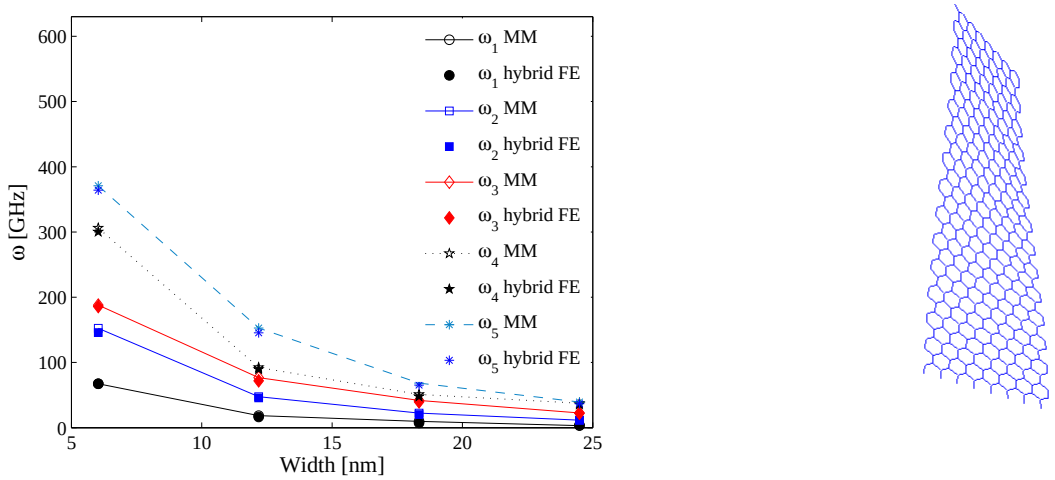


(a) (b)

Figure 1: Free-free vibration of SLGS nanoribbons. (a) Comparison between MM (black) and hybrid-FE (red) derived natural frequencies for (8,0) SLGSs with different lengths. (b) Mode shape # 2 for the SLGS with length 6.03 nm ($\omega$=145.6 GHz)

## 3. RESULTS AND DISCUSSIONS

Figure 1a shows the comparison between the MM simulations and the ones from the hybrid FE models for a (8,0) nanoribbon at different lengths (6.03 nm, 12.18 nm, 18.34 nm and 24.49 nm). The equilibrium lengths are $l = 0.142$ nm for all cases. For the flexural modes the hybrid FE approach identifies a bond thickness $d$ of 0.077 nm, with only a difference around 3 % when the first torsional mode is considered (Figure 1b). The identified thickness value compares well with the 0.074 nm - 0.099 nm found by the some of the Authors in uniaxial tensile loading,[11] the 0.0734 nm in uniaxial stretching using first generation Brenner potential,[34] and the 0.0894 nm of Kudin *et al* using *ab initio* techniques.[35] Gupta and Batra[36] identify a thickness of 0.080 nm for the $\omega_{11}$ frequency of a fully clamped SLGS (single layer graphene sheet) with dimensions 3.23 nm X 2.18 nm combining a MD simulation and results from continuum elasticity of plates. It is worth noticing that these results are significantly different from the usual 0.34 nm interatomic distance adopted by the vast majority of the community in nanomechanical simulations. The percentage difference between our MM and hybrid FE natural frequencies is on average around 3 % for all the flexural modes. The torsional frequencies for the nanoribbons with the lowest aspect ratio provide a higher error ($\sim$ 5 %), suggesting that the assumption of equal in-plane and out-of-plane torsional stiffness with the AMBER model in Eq. (1) provides a slightly lower out-of-plane torsional stiffness of the nanoribbon.

The 1D wave propagation analysis has been carried out on (8,0) nanoribbons with a length of 15.854 nm along the zigzag direction, and 15.407 nm along the armchair direction for the (0,8) cases. The hybrid FE models have been subjected to simply supported (SS) conditions, clamping the relevant DOFs in the middle location of the ribbons, and allowing therefore to apply the relations (11) using a set of constraint equations. The wave dispersion characteristics for the propagation along the zigzag edge of the nanoribbons are shown in Figure (2a). The first four pass-stop bands are typical of periodic SS beams under bending deformation,[37] while the out-of-plane torsional modes appear for the $5^{th}$ and $6^{th}$ wave dispersion characteristics. The first four mode shapes for $k_x = \pi/4$ are shown in Figure 3. The SLGS deform as classical beams under flexure, further confirming the validity of considering the nanoribbons as one-dimensional elastic element under bending for the lowest modes. The continuous lines in Figure 2a are referred to the Hamiltonian minimized only versus the thickness $d$, for a constant equilibrium length of $l = 0.142$ nm. For all the flexural mode shapes, we have identified a constant value of $d = 0.077$ nm, while no specific dependence over the wave propagation constant $k_x$ has been observed. However, when including the distribution of the bond length $l$ within the minimisation of the Hamiltonian, the

wave dispersion characteristics tend to assume a different behaviour. Apart from the first flexural band, all the other characteristics are lowered in terms on frequency, with the discrepancies between 3 % and 4 % observed for the highest wave bands. For those configurations, the minimized thickness (0.076 nm) is only slightly different from the 0.077 nm of the other cases observed so far. However, the average bond length $l$ is now equal to 0.145 nm, always within the accepted equilibrium lengths in open literature.[11,12] The new average C-C bond length implies that the overall dimensions of the nanoribbon are modified, with a total length of 16.199 nm for the case considered.

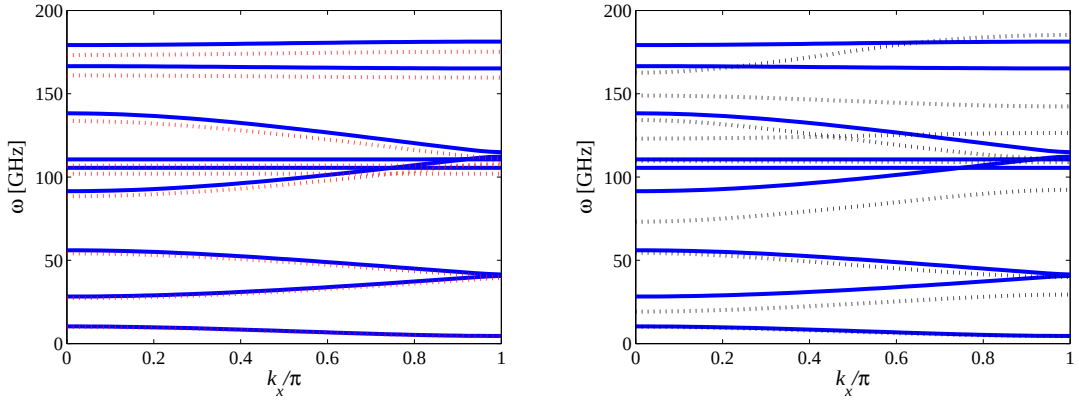


(a) (b)

Figure 2: Wave dispersion along the zigzag and armchair directions for a (8,0) GNR with length 15.854 nm.(a) Continuous line is referred to the Hamiltonian minimized versus $d$. Semicolon line is for the Hamiltonian minimized both for $d$ and $l$. (b) Comparison of wave dispersions along the zigzag direction (continuous line) and armchair (semicolon). The Hamiltonians are minimized for $d$ only.

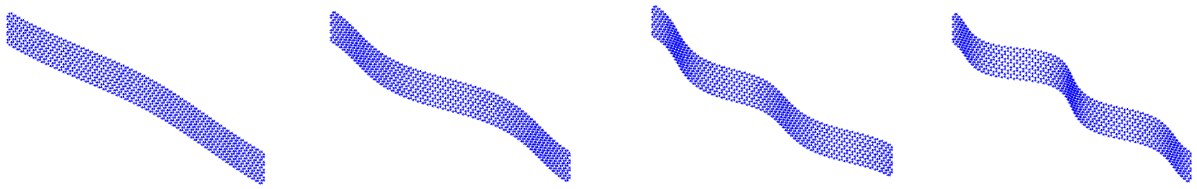

(a) $\omega_1$= 8.84 GHz (b) $\omega_2 = 29.35$ GHz (c) $\omega_3 = 52.5$ GHz (d) $\omega_3 = 92.5$ GHz

Figure 3: Mode shapes for a (8,0) GNR (length 15.854 nm) with propagation constant $k_x = \pi/4$ along the zigzag direction.

A more significant discrepancy between wave dispersion characteristics is observed when comparing the pass-stop band behaviour for the propagation along the zigzag and armchair directions (Figure 2b). Only the first flexural wave dispersion characteristic is virtually unchanged, while for the other characteristics we observe a strong decrease in terms of magnitude, as well as mode inversion. The first stop band is significantly decreased, with a final value of $\Delta\omega = 25.1$ GHz for $k_x = \pi$ - the armchair case gives a $\Delta\omega = 39$ GHz for the same propagation constant. Similar decreases in band gaps are observed for higher frequencies, while mode inversion (flexural to torsional) is observed for the armchair propagation around $k_x/\pi = 0.42$, while for the armchair case the mode inversion is located around 0.8 $k_x/\pi$. From the mechanical point of view, a possible explanation for this peculiar behaviour can be given considering the intrinsic anisotropy of the in-plane properties of finite size graphene sheets. Reddy and co-workers[14,38] have observed anisotropy ratios between 0.92 and 0.94 in almost square graphene

sheets subjected to uniaxial loading, while similar orthotropic has been identified also by Scarpa *et al.*[11] The GNRs considered here have an aspect ratio close to 6, giving the particular edges a higher contribution to the homogenised mechanical properties due to Saint Venant effects.[39] It appears also that specific morphology of the edges affect the wave propagation characteristics, and the widening of the band gap observed in Figure 2b recalls some similarity to the increase of the energy gap of the electronic states in armchair GNRs.[3]

## 4. CONCLUSIONS

We have presented a methodology to derive the structural dynamics characteristics and wave dispersion relations for graphene nanoribbons using an hybrid Finite Element approach. The technique, benchmarked ahainst a Molecular Mechanics model, allows to identify natural frequencies, modes shapes, and the pass-stop band characteristics of periodic arrays of GNRs. The numerical results from the minimisation of the Hamiltonian in the hybrid FE show that the commonly used value in nanomechanical simulations for the thickness (0.34 nm) is not adequate to represent the effective structural dynamics of the system. GNRs show a significant dependence of the wave propagation properties over the type of their edge, quite similarly to what observed for their electronic state. This feature suggests a possible combined electro-mechanical approach to design multifunctional waveguide-type band filters and mass sensors with enhanced selectivity.

## REFERENCES


1. Nakada K, Fujita M, Dresselhaus G, Dresselhaus M S, Edge state in graphene nanoribbons: Nanometer size effect and edge shape dependence, Phys. Rev. B 54 (24) (1996) 17954.
2. Wang Z F, Shi Q W, Li Q, Wang X, Hou J C, Z-shaped graphene nanoribbon quantum dot device, App. Phys. Lett. 91 (2007) 053109.
3. Barone V, Hod O, Scuseria G V, Electronic Structure and Stability of Semiconducting Graphene Nanoribbons, Nano Lett. 6 (12) (2006) 2748.
4. Han M Y, Ozyilmaz B, Zhang Y, Kim P, Energy Band-Gap Engineering of Graphene Nanoribbons, Phys. Rev. Lett. 98 (20) (2007) 206805 1 – 206805 4.
5. Law, Matt and Sirbuly, Donald J. and Johnson, Justin C. and Goldberger, Josh and Saykally, Richard J. and Yang, Peidong, Nanoribbon Waveguides for Subwavelength Photonics Integration, Science 305 (5688) (2004) 269.
6. Yosevich Y A, Savin A V, Reduction of phonon thermal conductivity in nanowires and nanoribbons with dynamically rough surfaces and edges, Eur. Phys. Lett. 88 (2009) 14002.
7. Ruzzene M, Baz A, Attenuation and localization of wave propagation in periodic rods using shape memory inserts, Smart Mat. Struct. 9 (2000) 805.
8. Gonella S, Ruzzene M, Homogenization of vibrating periodic lattice structures, App. Math. Modelling 32 (4) (2008) 459.
9. Tee K F, Spadoni A, Scarpa F, Ruzzene M, Wave propagation in auxetic tetrachiral honeycombs, J. Vib. Acoust.doi:10.1115/1.4000785.
10. Kempa K., Kimball B, Rybczynski J, Huang Z. P, Wu P. F, Steeves D, Sennett M, Giersig M, Rao D. V. G. L. N, Carnahan D. L, Wang D. Z, Lao J. Y, Li W. Z, Ren Z. F, Photonic Crystals Based on Periodic Arrays of Aligned Carbon Nanotubes, Nano Lett. 3 (1) (2003) 13.
11. Scarpa F, Adhikari S, Phani A S, Effective elastic mechanical properties of single layer graphene sheets, Nanotechnology 20 (2009) 065709.
12. Scarpa F, Adhikari S, Gil A J, Remillat C, The bending of single layer graphene sheets: Lattice versus continuum approach, Nanotechnology. Accepted.
13. Scarpa F, Adhikari S, A mechanical equivalence for Poisson's ratio and thickness of C-C bonds in single wall carbon nanotubes, J. Phys. D: App. Phys. 41 (8) (2008) 085306.
14. Reddy C D, Rajendran S, Liew K M, Equilibrium configuration and elastic properties of finite graphene, Nanotechnology 17 (2006) 864.
15. Reddy C D, Ramasubramaniam A, Shenoy V B, Zhang Y W, Edge elastic properties of defect-free single-layer graphene sheets, App. Phys. Lett. 94 (10) (2009) 101904.

16. Sun C Q, Sun Yi, Nie Y G, Wang Y, Pan J S, Ouyang G, Pan L K, Sun Z, Coordination-Resolved C-C Bond Length and the C1s Binding Energy of Carbon Allotropes and the Effective Atomic Coordination of the Few-Layer Graphene, J. Phys. Chem. C 113(37) (2009) 16464.
17. Sakhaee-Pour A, Ahmadian M T, Vafai A, Potential application of single-layered graphene sheet as strain-sensor, Solid State Comm. 147 (7-8) (2008) 336–340.
18. Sakhaee-Pour A, Ahmadian M T, Naghdabadi R, Vibrational analysis of single-layered graphene sheets, Nanotechnology 19 (2008) 085702.
19. Sakhaee-Pour A, Elastic properties of single-layered graphene sheet, Solid State Comm. 149 (1-2) (2009) 91.
20. Tserpes K I, Papanikos P, Finite Element modelling of single-walled carbon nanotubes, Comp. B 36 (2005) 468.
21. Ponte Castaneda P, Willis J R, The Effect of Spatial Distribution on the Effective Behavior of Composite Materials and Cracked Media, J. Mech. Phys. Solids 43 (1995) 1919.
22. Bornert M, Bretheau T, Gilormini P, Homogenization in Mechanics of Materials, Wiley-Iste, 2008.
23. Timoshenko S, Theory of Plates and Shells, McGraw-Hill, Inc, London, 1940.
24. Kaneko T, On Timoshenko's correction for shear in vibrating beams, J. Phys. D: App. Phys. 8 (1974) 1927.
25. Przemienicki J S, Theory of Matrix Structural Analysis, McGraw-Hill, New York, 1968.
26. Li C, Chou T W, Single-walled carbon nanotubes as ultrahigh frequency nanomechanical resonators, Phys. Rev. B 68 (2003) 073405.
27. Rajendran S, Reddy C D, Determination of Elastic Properties of Graphene and Carbon-NanotubesUsing Brenner Potential: The Maximum Attainable Numerical Precision, J. Comp. Theoret. Nanosci. 3 (2006) 1.
28. Goldstein H, Poole C P, Safko J L, Classical Mechanics, Addison-Wesley, Cambridge, MA, 1950.
29. Friswell M I, Mottershead J E, Finite Element Updating in Structural Dynamics, Kluwer Academic Publishing, 1995.
30. Chowdhury R, Adhikari S, Scarpa F, Vibrational analysis of ZnO nanotubes, Nanotechnology. Submitted.
31. Rappe A K, Casewit C J, Colwell K S, Goddard W A, Skiff W M, UFF, a full periodic-table force-field for molecular mechanics and molecular dynamics simulations, J. Am. Chem. Soc. 114 (25) (1992) 10024.
32. Aberg M, Gudmundson P, The Usage of Standard Finite Element Codes for Computation of Dispersion Relations in Materials With Periodic Microstructure, J. Acoust. Soc. Ame. 102 (4) (1997) 2007.
33. Brillouin L, Wave Propagation in Periodic Structures, Dover Phoenix Editions, 1953.
34. Huang Y, Wu J, Hwang K C, Thickness of graphene and single wall carbon nanotubes, Phys. Rev. B 74 (2006) 245413.
35. Kudin K N, Scuseria G E, Yakobson B I, C2F, BN and C nanoshell elasticity from ab initio computations, Phys. Rev. B 64 (2001) 235406.
36. Gupta S S, Batra R C, Elastic properties and frequencies of single-layer graphene sheets, J. Comp. Theor. Nanosci. Accepted.
37. Mead D J, Free wave propagation in periodically supported, infinite beams, J. Sound Vib. 11 (2) (1970) 181.
38. Reddy C D, Rajendran S, Liew K M, Equivalent Continuum Modeling of Graphene Sheets, Int. J. Nanosci. 4 (4) (2005) 631.
39. Horgan C O, Recent developments concerning Saint Venant's principle: an update, Appl. Mech. Rev. 42 (1989) 295.